In: 2022 American Control Conference (ACC), 8-10 June 2022, Atlanta, USA
DOI:10.23919/ACC53348.2022.9867858

Real-Time Path-tracking MPC for an Over-Actuated Autonomous Electric Vehicle

Chenhui Lin[1], Efstathios Siampis[2] and Efstathios Velenis[3]

***Abstract*— This paper illustrates the development of a nonlinear constrained predictive path-tracking controller, including realistic vehicle dynamics and multiple actuator inputs and its implementation in real time on an experimental vehicle platform. The controller is formulated for a particular over-actuated vehicle equipped with Torque Vectoring (TV) as well as All-Wheel-Steering (AWS) functionalities, which allow for the enhanced control of vehicle dynamics. The proposed Nonlinear Model Predictive Controller (NMPC) takes into account the nonlinearities in vehicle dynamics across the range of operation up to the limits of handling as dictated by the adhesion limits of the tyres. In addition, crucial constraints regarding the actuators' physical limits are included in the formulation. The performance of the controller is demonstrated in a high fidelity simulation environment, as well as in real-time on a test vehicle, during the execution of demanding driving scenarios.**

I. INTRODUCTION

Several active chassis control systems, such as Torque-Vectoring (TV) [1], [2], [3] and All-Wheel-Steering (AWS), which exploit the additional actuation available in modern vehicles, have enabled driver assist functionalities for the enhancement in safety and driver experience. In the context of highly automated driverless vehicles the available multi-actuation can be deployed to deliver enhanced performance of the autonomous driving controller, especially at the path tracking layer under demanding driving conditions.

There is a plethora of approaches to address the path tracking task. Recently model based control approaches have received attention for their capability of incorporating important features of the vehicle dynamics as well as multi-variable control formulations. The path-tracking control performance of different controllers including geometric controller, linear quadratic regulator and MPC were compared [4]. Simulation results showed that MPC achieved the best tracking performance with the minimum control effort. Futhermore, MPC has shown its advantage in dealing with constraints such as state and input limits [5] or road boundaries [6]. Hence, MPC has been widely utilized for autonomous vehicle control, especially for the path-tracking problem [7], [8], [9], [10], [11]. In [10], longitudinal dynamics of the vehicle was neglected with the assumption of a constant velocity, and thus the controller was based on a simplified linear system with linear tyre model. Liniger et al. proposed a predictive reference tracking controller for autonomous racing, and a predictive contouring controller which integrated path-planning and path-tracking [11]. Both controllers were based on linear time-varying (LTV) approximation of the system dynamics. In the above studies, linearization of the vehicle dynamics models, as well as the tyre models, are carried out to reduce the computational complexity of MPC. However, such simplification may no longer be sufficient to guarantee good prediction of the vehicle dynamics if multi-actuation is applied or during the operation at the limits of handling, when the vehicle behaviour becomes highly nonlinear.

Recently the inclusion of multi-actuation capabilities of modern vehicles in the path tracking control formulation has been discussed in the literature. Chatzikomis et al. compared a selection of path-tracking controllers with and without the TV functionality, and the results confirmed that TV control could effectively improve the cornering response at the limits of handling by generating a direct yaw moment to stabilize the vehicle [12]. Guo et al. presented a real-time implementable path-tracking controller based on MPC [13]. The controller applied an LTV system and was in the hierarchical structure, with the upper level determining the FWS angle as well as required yaw moment, and the lower level achieving that requirement through control allocation. In [14], a path-tracking controller for four-wheel drive (4WD) and AWS vehicles was developed. The controller was based on linear vehicle and tyre models, and a similar hierarchical structure. The disadvantage of such formulation was the exclusion of steering from control allocation. In addition, as the higher level of the control structure was based on linear system, it is hard to guarantee performance in extreme, near limit of handling conditions. Acosta et al. proposed a multi-actuation controller based on nonlinear vehicle and tyre models for autonomous drift control [15]. The work demonstrated the potential of combined FWS and TV to exploit the vehicle's dynamical capability. However, path-tracking was excluded from the MPC strategy, and was carried out by a PID controller. In addition, the controller has not been implemented in real-time.

In this work we present a real-time applicable nonlinear predictive path tracking control, designed to address demanding near limit-of-handling conditions, which takes into account the available TV and AWS capabilities of a modern vehicle. The rest of the paper is organised as follows. Section II introduces the modelling of vehicle dynamics. Then the optimal control problem is formulated in Section III. Section

This work was supported by Innovate UK (Project Reference: 104277).

[1]C. Lin is with the Advanced Vehicle Engineering Centre, School of Aerospace, Transport and Manufacturing, Cranfield University, Cranfield, MK43 0AL, UK. Chenhui.Lin@cranfield.ac.uk

[2]E. Siampis is with the Advanced Vehicle Engineering Centre, School of Aerospace, Transport and Manufacturing, Cranfield University, Cranfield, MK43 0AL, UK Efstathios.Siampis@cranfield.ac.uk

[3]E. Velenis is with the Advanced Vehicle Engineering Centre, School of Aerospace, Transport and Manufacturing, Cranfield University, Cranfield, MK43 0AL, UK e.velenis@cranfield.ac.uk

IV presents the simulation and vehicle test results followed by the conclusions.

II. MODELLING

Figure 1 shows the actuator topology of the vehicle under consideration. It is an EV prototype with 4WD and AWS functionality, realised using three electric motors (motor M1 driving the front wheels through an open differential, while the rear wheels are respectively driven by the other two motors M2 and M3) and two steer-by-wire systems, one per axle. It should be mentioned at this point that the control strategy designed here for this specific vehicle is extendable to fit most kind of multi-actuation configuration of EVs.

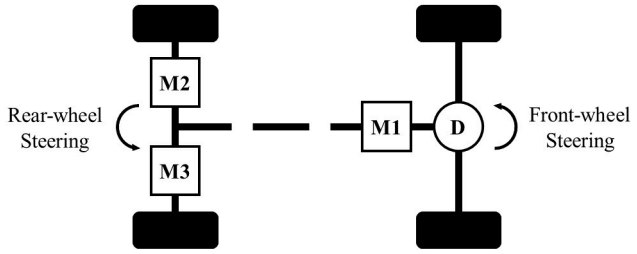

Fig. 1. Actuator topology of the case study vehicle.

A. Equations of Motion

A two-track vehicle model is used for the design of the path-tracking controller. The model is formulated around the vehicle's centre of gravity (CoG), and with assumptions that the vehicle travels on a horizontal plane, while the pitch, roll and heave motion are neglected. The model is shown in Figure 2, and the equations of motion are given as follows:

$$\begin{aligned} m(\dot{V}_x - V_y r) = \; & (F_{FLx} + F_{FRx})\cos\delta_F \\ & -(F_{FLy} + F_{FRy})\sin\delta_F \\ & +(F_{RLx} + F_{RRx})\cos\delta_R \\ & -(F_{RLy} + F_{RRy})\sin\delta_R \end{aligned} \tag{1}$$

$$\begin{aligned} m(\dot{V}_y + V_x r) = \; & (F_{FLx} + F_{FRx})\sin\delta_F \\ & -(F_{FLy} + F_{FRy})\cos\delta_F \\ & +(F_{RLx} + F_{RRx})\sin\delta_R \\ & -(F_{RLy} + F_{RRy})\cos\delta_R \end{aligned} \tag{2}$$

$$\begin{aligned} I_z\dot{r} = \; & l_F \cdot (F_{FLx} + F_{FRx})\sin\delta_F \\ & +l_F \cdot (F_{FLy} + F_{FRy})\cos\delta_F \\ & -l_R \cdot (F_{RLx} + F_{RRx})\sin\delta_R \\ & -l_R \cdot (F_{RLy} + F_{RRy})\cos\delta_R \\ & -w_L \cdot (F_{FLx}\cos\delta_F - F_{FLy}\sin\delta_F) \\ & -w_L \cdot (F_{RLx}\cos\delta_R - F_{FLy}\sin\delta_R) \\ & +w_R \cdot (F_{FRx}\cos\delta_F - F_{FRy}\sin\delta_F) \\ & +w_R \cdot (F_{RRx}\cos\delta_R - F_{RRy}\sin\delta_R) \end{aligned} \tag{3}$$

In the above equations, V_x and V_y are the longitudinal and lateral velocity at CoG, and r is the yaw rate. The vehicle's mass is represented by m, and I_z is the vehicle's moment of inertia about the vertical axis through CoG. The dimensions of the vehicle are given by l_F and l_R, which stand for the distances from CoG to the front and rear axle, and by w_L and w_R, which stand for the left and right portions of the track width divided by CoG. The longitudinal and lateral tyre forces are denoted by F_{ijk} $(i = F, R,\ j = L, R,\ k = x, y)$. Finally, δ_F and δ_R denotes the steering angles respectively on the front and rear wheels.

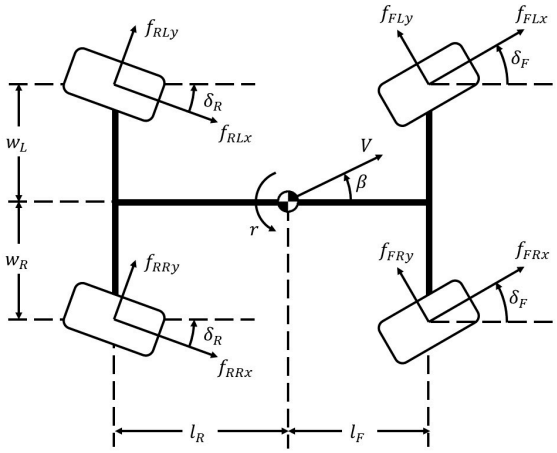

Fig. 2. Schematic diagram of the vehicle model.

In this paper, global coordinates are used to identify the vehicle position, and the derivatives of the vehicle position as well as yaw angle Ψ can be calculated as:

$$\dot{X} = V_x\cos(\Psi) - V_y\sin(\Psi) \tag{4}$$

$$\dot{Y} = V_x\sin(\Psi) + V_y\cos(\Psi) \tag{5}$$

$$\dot{\Psi} = r \tag{6}$$

B. Tyre Model

The behaviour of vehicle dynamics is highly nonlinear near the limits of handling due to the nonlinearities in the tyre force characteristics. Thus, an appropriate tyre force model is crucial for the control design in such operating conditions. With the assumption of neglecting the pitch, roll and vertical motion of the sprung mass of the vehicle, the vertical loads at each wheel can be calculated according to the static vertical load and the transferred weight corresponding to the longitudinal and lateral acceleration. The total vertical load at each wheel F_{ijz} are given by:

$$F_{FLz} = F_{FLz0} + \frac{mh}{lw}\cdot(-w_R a_x - l_R a_y) \tag{7}$$

$$F_{FRz} = F_{FRz0} + \frac{mh}{lw}\cdot(-w_L a_x + l_R a_y) \tag{8}$$

$$F_{RLz} = F_{RLz0} + \frac{mh}{lw}\cdot(w_R a_x - l_F a_y) \tag{9}$$

$$F_{RRz} = F_{RRz0} + \frac{mh}{lw}\cdot(w_L a_x - l_F a_y), \tag{10}$$

where a_x and a_y are the longitudinal and lateral acceleration of the vehicle, and h denotes the height of CoG from the ground. F_{ijz0} are the static vertical force on each wheel.

The slip angles on the front and rear tyres can be calculated by the following equations. It is assumed that the slip angles are the same at left and right tyres.

$$\alpha_F = \arctan \frac{V_y + l_F \cdot r}{V_x} - \delta_F \tag{11}$$

$$\alpha_R = \arctan \frac{V_y - l_R \cdot r}{V_x} - \delta_R \tag{12}$$

Assuming that the tyre does not exceed the adhesion limit in the longitudinal direction, which can be enforced through an appropriate constraint in the control formulation, allows us to neglect the wheel rotational dynamics [16]. In this case, the tyre longitudinal force is proportional to the applied driving or braking torque on the wheel. As introduced in the previous section, the front wheels are driven by a single motor through the differential, it is assumed that the torque on the front axle is evenly distributed on the two front wheels. By introducing the three control inputs T_F, T_{RL} and T_{RR}, the longitudinal tyre force on each wheel can be calculated as follows:

$$F_{Fjx} = \frac{T_F/2}{R_w} \tag{13}$$

$$F_{Rjx} = \frac{T_{Rj}}{R_w} \tag{14}$$

The lateral tyre force on individual wheels can be calculated as a function of the tyre slip angle through the simplified Pacejka Magic Formula tyre model [17]

$$F_{ijy} = -F_{ijz} \cdot D \sin\left(C \arctan\left(B\alpha_i\right)\right) \tag{15}$$

III. PREDICTIVE PATH-TRACKING CONTROLLER

The nonlinear continuous-time system can be described as:

$$\dot{x}_t = fc(x_t,\ u_t), \tag{16}$$

where x_t stands for the state vector $[V_x, V_y, r, X, Y, \Psi]^T$ and u_t refers to the control input vector $[\delta_F, \delta_R, T_F, T_{RL}, T_{RR}]^T$.

The controller is realised in the sampled-data framework by discretizing the nonlinear continuous-time system dynamics using the explicit Runge-Kutta 4th order method, with f_d the discrete-time equivalent of the original system f_c. The discrete NMPC problem is formulated as

$$\begin{aligned} \min_{x,u} \ & \sum_{k=0}^{N-1} (x_{k+1} - x_{ref,k+1})^T Q (x_{k+1} - x_{ref,k+1}) \\ & + {u_k}^T R u_k \\ st. \ \ & x_0 = x_{initial} \\ & x_{k+1} = f_d(x_k, u_k), k = 0, \cdots, N-1 \\ & u_{min} \le u_k \le u_{max}, k = 0, \cdots, N-1 \end{aligned} \tag{17}$$

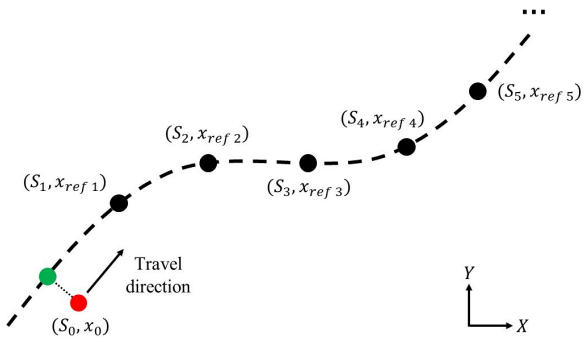

Fig. 3. Diagram of the reference waypoints. The red point represents the vehicle's position, while the green point stands for the projection of vehicle position on the reference path. The interval of the waypoints $\Delta S = V_{ref} \cdot t_s$, where V_{ref} is the reference velocity and t_s is the sampling time of the controller.

where N is the steps in the prediction horizon, x_{ref} is the reference state vector and Q, R are the weighting matrices of the state and control input errors respectively. For limiting the control inputs, box constraints are utilised.

The reference path is parametrized by the arc length S along the path starting from the origin point, where $S \in [0, L]$ and L is the total length of the path. With this parameterization, the position $X_{ref}(S), Y_{ref}(S)$ of any point on the reference path can be obtained by calculating the third order polynomial for the argument S. In addition, the tangential angle of the path at the point can be obtained as

$$\Psi_{ref}(S) = \arctan \frac{\partial Y_{ref}(S)}{\partial X_{ref}(S)}, \tag{18}$$

and is used as the reference yaw angle of the vehicle. This parameterization takes advantage of the known waypoints on the reference path and provides an accurate enough interpolation within them [11].

Using the projection point $(X_{ref}(S_0), Y_{ref}(S_0))$ of the vehicle position on the reference path, S_0 can be obtained by solving the minimum distance problem

$$S_0 = \min_S \ [X - X_{ref}(S)]^2 + [Y - Y_{ref}(S)]^2. \tag{19}$$

S_0 can be used to denote the progress of the vehicle along the reference path, and the distance between the vehicle and this projection point refers to the lateral deviation of the vehicle from the path. In order to reduce the computational time, the above minimum distance problem is solved only for points in the path closest to the current position.

For the discrete objective function, a total of N waypoints are required to generate x_{ref}, starting from $(X_{ref}(S_0), Y_{ref}(S_0))$. The distance between the waypoints is then given by

$$\Delta S = S_{k+1} - S_k = V_{ref} \cdot t_s, k = 0, \cdots, N-1 \tag{20}$$

where V_{ref} is the reference velocity and t_s is the sampling time of the discrete-time system (Figure 3). The complete reference state vector x_{ref} is then evaluated by carrying out

TABLE I
PARAMETERS OF THE VEHICLE MODEL

Parameter (Unit)	Value	Parameter (Unit)	Value
m (kg)	974.5	B	9.500
I_z (kg m^2)	1597.7	C	1.626
l_F (m)	0.815	D	1.166
l_R (m)	1.180	δ_F limit (deg)	20
w_L (m)	0.765	δ_F limit (deg)	20
w_R (m)	0.765	T_F limit (Nm)	1600
h (m)	0.297	T_{RL} limit (Nm)	800
R_w	0.315	T_{RR} limit (Nm)	800

a third order spline polynomial based on the argument S. For solving the resulting optimisation problem, we use FORCES PRO from Embotech [18].

IV. RESULTS

In the following section, we demonstrate the path-tracking performance of the controller in simulation and on a test vehicle (vehicle parameters found in Table I) around a small track, consisting of several straight, U-turn and lane change sections. For the high-fidelity simulation results we use IPG CarMaker (CM), running on a workstation laptop (Intel Core i7-8750H CPU at a base frequency of 2.2GHz and 32GB RAM of memory). The test vehicle is equipped with the following devices: 1) a Speedgoat Mobile Real-Time Machine for deploying and running the developed control algorithm, 2) an OxTS RT1003 Dual-Antenna GPS system for tracking the vehicle response and 3) a dSpace MicroAutoBox II, which acts as the central Control Unit and is responsible for monitoring the vehicle status, providing information to the Speedgoat Mobile and passing its control commands back to the actuators (Figure 4). For both simulation and experimental results, the reference velocity is set to a constant value of 7.5m/s.

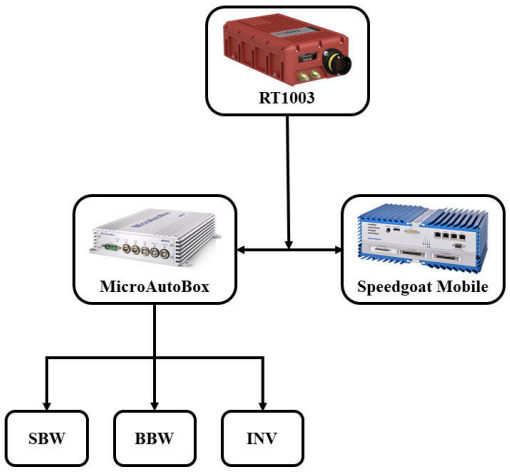

Fig. 4. Hardware topology of the testing vehicle for data processing.

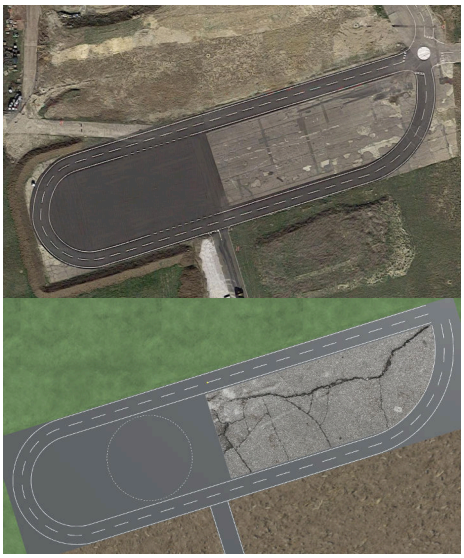

Fig. 5. Satellite birdview of the MUEAVI testing area where the experiments took place and its model in CM.

From Figure 6 we can see that the controller is able to closely track the reference path in simulation and most of the experiment, while keeping the velocity close to its reference value (Figure 7). The larger deviation from the path in the experimental results at the exit of the lane change section can be also confirmed in the lateral tracking error (Figure 9) and is linked to the larger lateral acceleration which reaches the friction limit at this point (Figure 8). The sideslip angle (Figure 8) shows a similar trend, while the yaw rate is more closely matched between simulation and experiment as can be seen in Figure 11.

From Figures 12-16 we can see that the control commands are also similar between the simulation and the experiment. The front and rear steering closely match, while the torques at the rear axle show some fluctuations in the commands towards the end of the experiment, which subsequently lead to the larger lateral tracking error at the exit of lane change. Finally, the computational time in both simulation and experiment is well within the sampling time of 100ms, as seen in Figure 17.

From the above results, we can confirm the controller's performance in both simulation and experiment, proving also its real-time implementability. Some discrepancy in the experimental results has been observed, which can be due to several factors such as uncertainties in the tyre-road friction coefficient and parametrisation of the tyre model in CM.

V. CONCLUSIONS

In this paper we present a novel path-tracking controller for an multi-actuated autonomous EV equipped with 4WD and 4WS capabilities. The controller design was based on an NMPC framework, using a nonlinear vehicle dynamics model appropriate for limit handling conditions and incorporating the necessary control limits.

The controller performance has been successfully validated across the range of operation up to the limits of

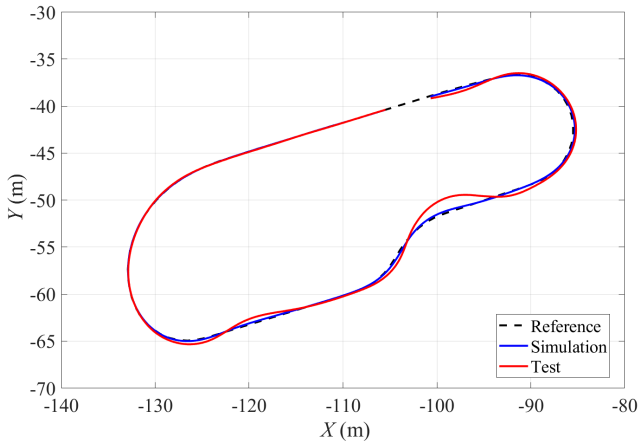

Fig. 6. Vehicle trajectory

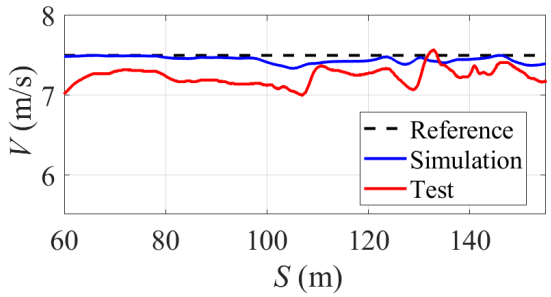

Fig. 7. Velocity

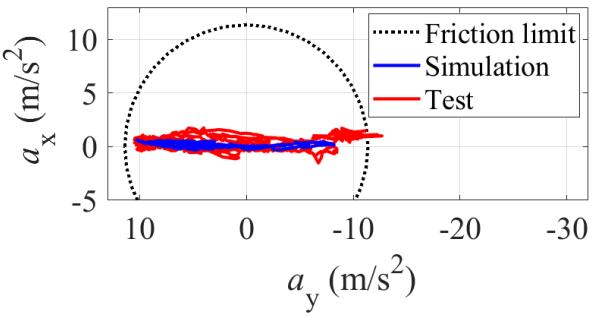

Fig. 8. g-g diagram

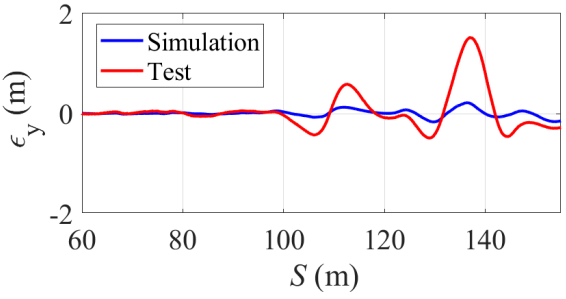

Fig. 9. Lateral tracking error

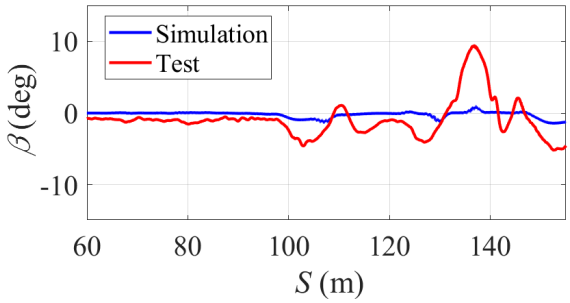

Fig. 10. Side slip angle

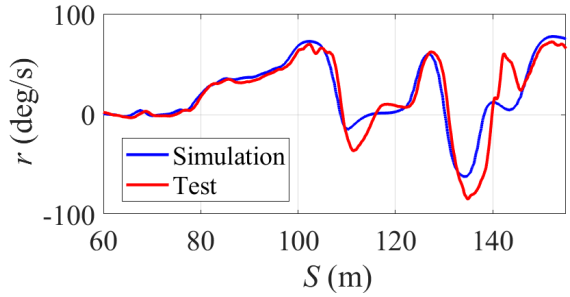

Fig. 11. Yaw rate

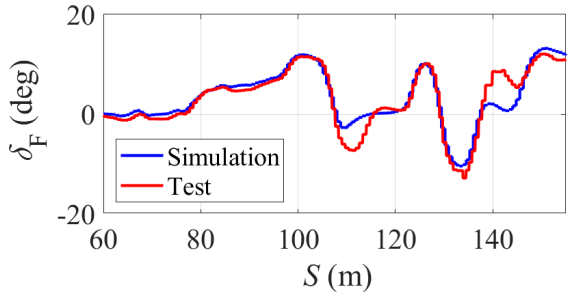

Fig. 12. Front steering commands

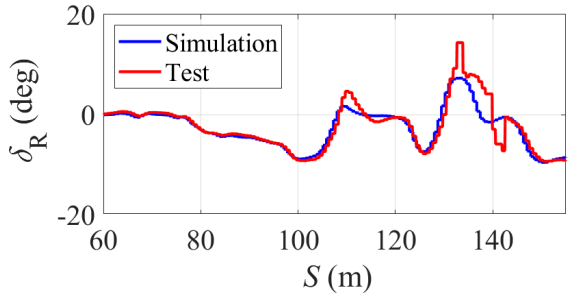

Fig. 13. Rear steering commands

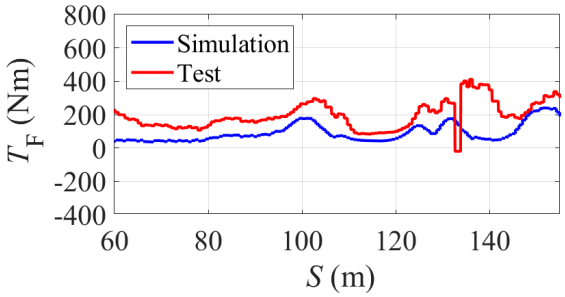

Fig. 14. Front wheel torque commands.

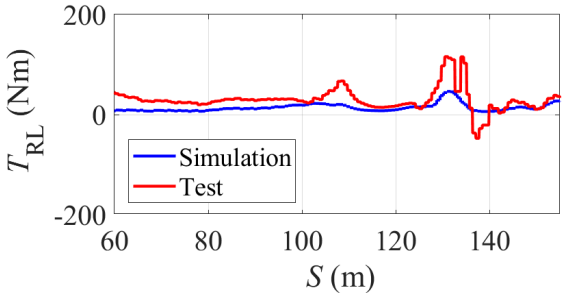

Fig. 15. Rear left wheel torque commands.

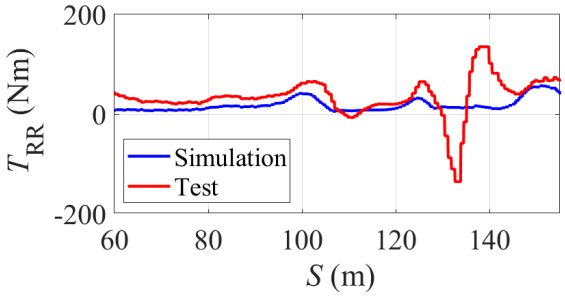

Fig. 16. Rear right wheel torque commands.

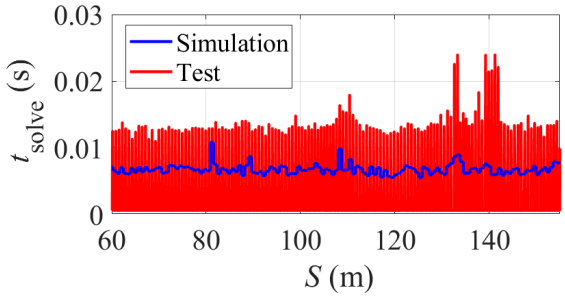

Fig. 17. Computational time

handling, with simulation and real-time test results on a prototype vehicle showing good agreement. In future work, we will aim at improving the tracking performance of the controller by incorporating more realistic reference values for states such as the sideslip angle and the velocity, also introducing a tyre-road friction coefficient estimator.

REFERENCES

[1] E. Siampis, E. Velenis, and S. Longo, "Model predictive torque vectoring control for electric vehicles near the limits of handling," in *2015 European Control Conference (ECC)*, July 2015, pp. 2553–2558.

[2] G. Vasiljevic and S. Bogdan, "Model predictive control based torque vectoring algorithm for electric car with independent drives," in *2016 24th Mediterranean Conference on Control and Automation (MED)*, June 2016, pp. 316–321.

[3] E. Mikuláš, M. Gulan, and G. Takács, "Model predictive torque vectoring control for a formula student electric racing car," in *2018 European Control Conference (ECC)*, June 2018, pp. 581–588.

[4] V. K, M. A. Sheta, and V. Gumtapure, "A comparative study of stanley, lqr and mpc controllers for path tracking application (adas/ad)," in *2019 IEEE International Conference on Intelligent Systems and Green Technology (ICISGT)*, June 2019, pp. 67–71.

[5] C. E. Beal and J. C. Gerdes, "Model predictive control for vehicle stabilization at the limits of handling," *IEEE Transactions on Control Systems Technology*, vol. 21, no. 4, pp. 1258–1269, July 2013.

[6] S. A. Bonab and A. Emadi, "Optimization-based path planning for an autonomous vehicle in a racing track," in *IECON 2019 - 45th Annual Conference of the IEEE Industrial Electronics Society*, vol. 1, 2019, pp. 3823–3828.

[7] G. V. Raffo, G. K. Gomes, J. E. Normey-Rico, C. R. Kelber, and L. B. Becker, "A predictive controller for autonomous vehicle path tracking," *IEEE Transactions on Intelligent Transportation Systems*, vol. 10, no. 1, pp. 92–102, March 2009.

[8] A. Alessandretti, A. P. Aguiar, and C. N. Jones, "Trajectory-tracking and path-following controllers for constrained underactuated vehicles using model predictive control," in *2013 European Control Conference (ECC)*, July 2013, pp. 1371–1376.

[9] H. Zhang, B. Heng, and W. Zhao, "Path tracking control for active rear steering vehicles considering driver steering characteristics," *IEEE Access*, vol. 8, pp. 98 009–98 017, 2020.

[10] W. Kim, D. Kim, K. Yi, and H. J. Kim, "Development of a path-tracking control system based on model predictive control using infrastructure sensors," *Vehicle System Dynamics*, vol. 50, no. 6, pp. 1001–1023, 2012.

[11] A. Liniger, A. Domahidi, and M. Morari, "Optimization-based autonomous racing of 1:43 scale rc cars," *Optimal Control Applications and Methods*, vol. 36, no. 5, pp. 628–647, 2015.

[12] C. Chatzikomis, A. Sorniotti, P. Gruber, M. Zanchetta, D. Willans, and B. Balcombe, "Comparison of path tracking and torque-vectoring controllers for autonomous electric vehicles," *IEEE Transactions on Intelligent Vehicles*, vol. 3, no. 4, pp. 559–570, Dec 2018.

[13] J. Guo, Y. Luo, K. Li, and Y. Dai, "Coordinated path-following and direct yaw-moment control of autonomous electric vehicles with sideslip angle estimation," *Mechanical Systems and Signal Processing*, vol. 105, pp. 183 – 199, 2018.

[14] T. Chen, L. Chen, X. Xu, Y. Cai, and X. Sun, "Simultaneous path following and lateral stability control of 4wd-4ws autonomous electric vehicles with actuator saturation," *Advances in Engineering Software*, vol. 128, pp. 46–54, 2019.

[15] M. Acosta, S. Kanarachos, and M. E. Fitzpatrick, "On full magv lateral dynamics exploitation: Autonomous drift control," in *2018 IEEE 15th International Workshop on Advanced Motion Control (AMC)*, March 2018, pp. 529–534.

[16] K. Zarkadis, E. Velenis, E. Siampis, and S. Longo, "Predictive torque vectoring control with active trail-braking," in *2018 European Control Conference (ECC)*, June 2018, pp. 569–574.

[17] H. B. Pacejka and E. Bakker, "The magic formula tyre model," *Vehicle System Dynamics*, vol. 21, no. sup001, pp. 1–18, 1992.

[18] A. Domahidi and J. Jerez, "Forces professional," Embotech AG, url=https://embotech.com/FORCES-Pro, 2014–2019.

Real-time path-tracking MPC for an over-actuated autonomous electric vehicle

Lin, Chenhui

2022-09-05

Lin C, Siampis E, Velenis E. (2022) Real-time path-tracking MPC for an over-actuated autonomous electric vehicle. In: 2022 American Control Conference (ACC), 8-10 June 2022, Atlanta, USA

https://doi.org/10.23919/ACC53348.2022.9867858